

Indirect neural-based finite-time integral sliding mode control for trajectory tracking guidance of Mars entry vehicle

Qijia Yao^{a,b,*}, Hadi Jahanshahi^c, Irene Moroz^d, Stelios Bekiros^e, Madini O. Allassafi^f

^a School of Automation and Electrical Engineering, University of Science and Technology Beijing, Beijing 100083, China

^b School of Aerospace Engineering, Beijing Institute of Technology, Beijing 100081, China

^c Department of Mechanical Engineering, University of Manitoba, Winnipeg R3T 5V6, Canada

^d Mathematical Institute, University of Oxford, Oxford OX2 6GG, UK

^e FEMA, University of Malta, MSD 2080 Msida, Malta

^f Department of Information Technology, Faculty of Computing and Information Technology, King Abdulaziz University, Jeddah 21589, Saudi Arabia

Received 27 May 2022; received in revised form 8 November 2022; accepted 29 November 2022

Available online 6 December 2022

Abstract

This article presents an indirect neural-based finite-time integral sliding mode control algorithm for the reference trajectory tracking guidance of Mars entry vehicle under uncertainties. The proposed controller is developed as a combination of finite-time integral sliding mode controller and indirect neural identification. The finite-time integral sliding mode controller is designed by constructing a new type of finite-time integral sliding mode surface to prevent the singularity problem. Moreover, the neural network (NN) is combined with the finite-time integral sliding mode controller to identify the lumped uncertainty and attenuate the chattering phenomenon. Particularly, the concept of indirect neural identification is adopted and only a single adaptive parameter is required to be learned online. In this way, the proposed controller is not only strongly robust against aerodynamic and density uncertainties, but also computationally simple for onboard implementations. Stability argument indicates that the proposed controller can ensure the radial distance tracking error and its time differentiation regulate to the small residual sets around zero in finite time. Lastly, the effectiveness and excellent guidance performance of the proposed control algorithm are demonstrated through simulation studies on a Mars Science Laboratory-type (MSL-type) entry vehicle.

© 2022 COSPAR. Published by Elsevier B.V. All rights reserved.

Keywords: Reference trajectory tracking guidance; Mars entry vehicle; Finite-time control; Integral sliding mode control; Indirect neural identification

1. Introduction

As the nearest major planet to Earth, Mars is one of the primary targets for deep space exploration. Atmospheric entry guidance of entry vehicle is an important technology

for future manned Mars exploration and sample-return missions. On the one hand, the dynamic model of Mars entry vehicle is highly nonlinear and strongly coupled. On the other hand, the entry vehicle unavoidably suffers from aerodynamic and density uncertainties since the Mars atmospheric environment is complicated and changing. Consequently, the atmospheric entry guidance of Mars entry vehicle is a difficult problem for both aerospace engineering and control community (Braun and Manning, 2007; Li and Jiang, 2014; Yu et al., 2014).

Generally, the atmospheric entry guidance methods can be classified into the predictor–corrector guidance

* Corresponding author at: School of Automation and Electrical Engineering, University of Science and Technology Beijing, Beijing 100083, China.

E-mail addresses: qijia_yao@126.com (Q. Yao), irene.moroz@maths.ox.ac.uk (I. Moroz), stelios.bekiros@um.edu.mt (S. Bekiros), malasafi@kau.edu.sa (M.O. Allassafi).

(Lu, 2008, 2014; Xia et al., 2015; Zheng et al., 2017; Zheng, 2019) and the reference trajectory tracking guidance. The predictor–corrector guidance is insensitive to initial state errors, but it requires relatively accurate dynamic model of Mars entry vehicle and Mars atmosphere model. Moreover, the iterative correction of bank angle in each sampling period needs a large amount of computational resource. Thus, the predictor–corrector guidance requires the entry vehicle to have the powerful onboard computational capability. Alternatively, the reference trajectory tracking guidance has a relatively simple structure and is strongly robust against aerodynamic and density uncertainties. Therefore, the reference trajectory tracking guidance has been recognized as a preferable choice for Mars entry vehicle. Some performance comparisons between the predictor–corrector guidance and the reference trajectory tracking guidance can be found in Kluever (2008).

During the last decades, many advanced control methods have been utilized for the reference trajectory tracking guidance of Mars entry vehicle. Bharadwaj et al. (1998) designed a trajectory tracking control law for entry vehicles through feedback linearization. In Tu et al. (2000), a drag-based predictive tracking guidance law was developed for high-precision Mars landing. Li and Peng (2012a) proposed a command generator tracker based direct model reference adaptive control algorithm for the tracking guidance of Mars atmospheric entry. In Xia et al. (2014), an active disturbance rejection control was presented for drag tracking of Mars entry guidance. Zheng and Cui (2015) designed a disturbance observer based sliding mode guidance law for Mars atmospheric entry under input saturation. In Lu et al. (2017), a high-precision Mars entry guidance and control approach was proposed via sliding mode control and extended state observer. Yan and Lyu (2019) developed a Mars entry guidance scheme by integrating the nonlinear model predictive control with an disturbance observer. Besides, the intelligent control is another efficient method for the reference trajectory tracking guidance of Mars entry vehicle owing to the powerful approximation capability of neural network (NN) and fuzzy logic system. Typical studies within the field of spacecraft intelligent guidance and control can be found in Izzo et al. (2019) and Shirobokov et al. (2021). Li and Peng (2012b) developed a NN based sliding mode variable structure controller for the trajectory tracking guidance of Mars entry vehicle under uncertainties. In Li and Jiang (2015), a robust Mars atmospheric entry guidance approach was designed based on the radial basis function NN (RBFNN) and second-order sliding mode control. Huang et al. (2019) presented an active fault-tolerant control algorithm for Mars entry by utilizing NN and structure adaptive model inversion. In Li et al. (2019), a fuzzy control scheme was proposed for the fault-tolerant tracking of Mars entry vehicle with disturbances and actuator failures. However, it should be pointed out that the intelligent control brings heavy computational burden to the Mars entry vehicle since the conventional neural or fuzzy identification

requires a large number of adaptive learning parameters to be adjusted online.

Nevertheless, the above controllers can only guarantee the asymptotic stability or at best exponential stability of the closed-loop system. Alternatively, the finite-time control can ensure the radial distance tracking error and its time derivative regulate to zero or the small residual sets around zero in finite time. Generally, the finite-time control methods can be classified into the homogeneous method, adding a power integrator technique, and terminal sliding mode control. However, it is well known that the homogeneous method and the adding a power integrator technique are insensitive to uncertainties and disturbances. Therefore, the terminal sliding mode control is the more suitable finite-time control method for the reference trajectory tracking guidance of Mars entry vehicle. Dai and Xia (2015) developed a finite-time guidance law for reference trajectory tracking of Mars entry vehicle based on the terminal sliding mode control and an extended state observer. In Zhao et al. (2015), a nonsingular terminal sliding mode controller was presented for the Mars entry trajectory tracking under parameter perturbations and external disturbances. Dai et al. (2017) designed a robust nonlinear compound controller for the Mars atmospheric entry guidance by integrating the terminal sliding mode control with a second-order differentiator. Subsequently, Shen et al. (2018b) proposed a new compound control method consisting of an adaptive nonsingular terminal sliding mode controller and an extended state observer. In Shen et al. (2018a, 2019), several adaptive nonsingular terminal sliding mode control schemes were presented for the Mars entry trajectory tracking with finite-time convergence. Long et al. (2020) designed a barrier Lyapunov function based terminal sliding mode controller for the trajectory tracking of Mars entry vehicle with input saturation. In Gong et al. (2020), a dual-loop guidance algorithm was carried out for the tracking guidance of Mars entry vehicle under control constraints. The nonsingular terminal sliding mode controller and the proportional-differential (PD) controller were utilized as the outer-loop and inner-loop controllers, respectively. However, the terminal sliding mode control has the inherent disadvantage of singularity problem. Although several singularity avoidance strategies have been developed, the singularity problem is still an open problem for terminal sliding mode control currently. Recently, Zhao et al. (2016) proposed a disturbance observer-based integral sliding mode control method for the drag-based finite-time trajectory tracking guidance of Mars entry vehicle under uncertainties. The integral sliding mode control method has no singularity problem by constructing the integral sliding mode surface based on the homogeneous method.

The above observations motivate our study. This article presents an indirect neural-based finite-time integral sliding mode control algorithm for the reference trajectory tracking guidance of Mars entry vehicle under uncertainties. The proposed controller is developed as a combination of

finite-time integral sliding mode controller and indirect neural identification. The practical finite stability of the whole closed-loop system is theoretically achieved. The proposed controller can ensure the radial distance tracking error and its time differentiation regulate to the small residual sets around zero in finite time. The main contributions of the proposed control algorithm are reflected in the following two aspects.

- The first novelty is constructing a new type of finite-time integral sliding mode surface, based on which the finite-time integral sliding mode controller is designed with no singularity problem. This overcomes a major drawback of the conventional terminal sliding mode control.
- The second novelty is introducing the concept of indirect neural identification, which only requires a single adaptive parameter to identify the lumped uncertainty. Benefiting from this design, the proposed controller is computationally simple for onboard implementations.

The rest of this article is outlined as follows. Section 2 describes the problem and gives some preliminaries. Section 3 presents the control design and stability argument. Section 4 formulates the simulation studies. Lastly, Section 5 concludes this research.

2. Problem description and preliminaries

2.1. Problem description

During the Mars atmospheric entry, the entry vehicle is considered to fly at a constant trim angle of attack and the bank angle is modulated as the command signal. Since the Mars atmospheric entry only lasts a very short period of time, the centripetal acceleration caused by Mars self-rotation can be neglected. Subsequently, the motion of equation of the Mars entry vehicle can be expressed as (Bharadwaj et al., 1998; Tu et al., 2000; Li and Peng, 2012a, 2012b)

$$\begin{cases} \dot{r} = V \sin \gamma, \\ \dot{\theta} = \frac{V \cos \gamma \sin \psi}{r \cos \lambda}, \\ \dot{\lambda} = \frac{V \cos \gamma \cos \psi}{r}, \\ \dot{V} = -D - g \sin \gamma, \\ \dot{\gamma} = \left(\frac{V}{r} - \frac{g}{V}\right) \cos \gamma + \frac{L}{V} \cos \sigma, \\ \dot{\psi} = \frac{V \cos \gamma \sin \psi \tan \lambda}{r} + \frac{L \sin \sigma}{V \cos \gamma}, \end{cases} \quad (1)$$

where r denotes the radial distance between the Mars center and the entry vehicle, θ and λ are the latitude and longitude of the entry vehicle, V denotes the velocity of the entry vehicle, γ is the flight path angle, ψ is the heading angle, σ is the bank angle, $g = \mu_M/r^2$ is the gravitational acceleration, and μ_M is the Martian gravitational constant. Moreover, L and D are the lift and drag accelerations of the entry vehicle, denoted as

$$\begin{cases} L = \frac{C_L \rho S V^2}{2m}, \\ D = \frac{C_D \rho S V^2}{2m}, \end{cases} \quad (2)$$

where C_L and C_D are the lift and drag coefficients, m and S are the mass and reference area of the entry vehicle, and ρ is the Martian atmospheric density. Adopting the exponential model, the Martian atmospheric density can be expressed as

$$\rho = \rho_s \exp(-h/h_s), \quad (3)$$

where $h = r - r_M$ is the flight altitude of the entry vehicle, r_M is the Mars radius, ρ_s denotes the atmospheric density on Martian surface, and h_s denotes the scale altitude for Martian atmospheric density.

Let r_d be the desired radial distance between the Mars center and the entry vehicle. Then, define $x_1 = r - r_d$ and $x_2 = \dot{r} - \dot{r}_d$ as the radial distance tracking error and its time differentiation. Then, the time differentiation of x_2 can be evaluated as

$$\begin{aligned} \dot{x}_2 = & \frac{V^2 \cos^2 \gamma}{r} - \frac{C_D \rho S V^2}{2m} \sin \gamma + \frac{C_L \rho S V^2}{2m} \cos \gamma \cos \sigma \\ & - \frac{\mu_M}{r^2} - \ddot{r}_d. \end{aligned} \quad (4)$$

Since the Mars atmospheric environment is complicated and changing, the entry vehicle unavoidably suffers from aerodynamic and density uncertainties. When considering these uncertainties, the lift and drag coefficients and the Martian atmospheric density can be rewritten as

$$\begin{cases} C_L = C_{L0} + \Delta C_L, \\ C_D = C_{D0} + \Delta C_D, \\ \rho = \rho_0 + \Delta \rho, \end{cases} \quad (5)$$

where C_{L0} , C_{D0} , and ρ_0 are the nominal aerodynamic coefficients and atmospheric density, and ΔC_L , ΔC_D , and $\Delta \rho$ are the aerodynamic and density uncertainties, respectively. The control command for the Mars entry vehicle is set as $u = \cos \sigma$. When considering the input constraint, the control command can be expressed as

$$u = \begin{cases} u_m, & u_c \geq u_m, \\ u_c, & -u_m \leq u_c < u_m, \\ -u_m, & u_c < -u_m, \end{cases} \quad (6)$$

where u_m is the maximum control command value. Then, (6) can be rewritten as

$$u = u_c + u_\Delta, \quad (7)$$

where u_Δ is the control command deviation. Without loss of generality, u_Δ is assumed to be bounded in this work. Substituting (5) and (7) into (4), we have

$$\begin{aligned} \dot{x}_2 = & \frac{V^2 \cos^2 \gamma}{r} - \frac{(C_{D0} + \Delta C_D)(\rho_0 + \Delta \rho) S V^2}{2m} \sin \gamma \\ & + \frac{(C_{L0} + \Delta C_L)(\rho_0 + \Delta \rho) S V^2}{2m} \cos \gamma (u_c + u_\Delta) - \frac{\mu_M}{r^2} - \ddot{r}_d \\ = & H u_c + F + \delta, \end{aligned} \quad (8)$$

where H and F are the model-based nonlinear terms, denoted as

$$H = \frac{C_{L0}\rho_0 S V^2}{2m} \cos \gamma, \quad (9)$$

$$F = \frac{V^2 \cos^2 \gamma}{r} - \frac{C_{D0}\rho_0 S V^2}{2m} \sin \gamma - \frac{\mu_M}{r^2} - \ddot{r}_d. \quad (10)$$

Moreover, δ is the lumped uncertainty, denoted as

$$\begin{aligned} \delta = & -\frac{(\rho_0 \Delta C_D + C_{D0} \Delta \rho + \Delta C_D \Delta \rho) S V^2}{2m} \sin \gamma \\ & + \frac{(\rho_0 \Delta C_L + C_{L0} \Delta \rho + \Delta C_L \Delta \rho) S V^2}{2m} \cos \gamma u_c \\ & + \frac{(C_{L0} + \Delta C_L)(\rho_0 + \Delta \rho) S V^2}{2m} \cos \gamma u_\Delta. \end{aligned} \quad (11)$$

Subsequently, the control-oriented model for the reference trajectory tracking guidance of Mars entry vehicle can be described as

$$\begin{cases} \dot{x}_1 = x_2, \\ \dot{x}_2 = H u_c + F + \delta. \end{cases} \quad (12)$$

The objective is designing the bank angle control command u_c for the Mars entry vehicle to ensure the radial distance tracking error x_1 and its time differentiation x_2 can regulate to the small residual sets around zero in finite time even under aerodynamic and density uncertainties.

2.2. Preliminaries

Lemma 1. (Bhat and Bernstein, 2000) Consider the nonlinear system:

$$\dot{x} = f(x), \quad f(0) = 0, \quad x \in \mathbb{R}^n. \quad (13)$$

If there exists a positive definite function $V(x)$ satisfying $\dot{V}(x) \leq -\kappa V^q(x)$, where $\kappa > 0$ and $0 < q < 1$, then system (12) is globally finite-time stable and $V(x)$ can regulate to zero in finite time. Moreover, the upper bound of the finite settling time is given as $T_s \leq \frac{V^{1-q}(0)}{\kappa(1-q)}$.

Lemma 2. (Yao, 2020) Consider system (12). If there exists a positive definite function $V(x)$ satisfying $\dot{V}(x) \leq -\kappa_1 V(x) - \kappa_2 V^q(x) + \vartheta$, where $\kappa_1 > 0$, $\kappa_2 > 0$, $0 < q < 1$, and $\vartheta > 0$, then system (12) is practically finite-time stable and $V(x)$ can regulate to the following small residual set around zero in finite time:

$$\mathcal{Q} = \left\{ V(x) \in \mathbb{R} \mid V(x) \leq \frac{\vartheta}{(1-\iota)\kappa_1} \right\}, \quad (14)$$

where $0 < \iota < 1$. Moreover, the upper bound of the finite settling time is given as $T_s \leq \frac{1}{\iota\kappa_1(1-q)} \ln \frac{\iota\kappa_1 V^{1-q}(0) + \kappa_2}{\kappa_2}$.

Lemma 3. (Sanner and Slotine, 1992) Consider a continuous nonlinear function $f(Z)$, it can be identified by an RBFNN as.

$$f(Z) = W^{*T} \Phi(Z) + \varepsilon(Z), \quad (15)$$

where $W^* \in \mathbb{R}^N$ is the optimal RBFNN weight, $\Phi(Z) = [\phi_1(Z), \dots, \phi_N(Z)]^T \in \mathbb{R}^N$ is the basis function vector, $\varepsilon(Z)$ is the identification error satisfying $|\varepsilon(Z)| \leq \bar{\varepsilon}$, $\bar{\varepsilon} > 0$, and N is the number of neurons. Moreover, $\phi_i(Z)$ is commonly selected as the Gaussian function:

$$\phi_i(Z) = \exp \left(-\|Z - c_i\|^2 / w_i^2 \right), \quad i = 1, 2, \dots, N, \quad (16)$$

where $c_i = [c_{i,1}, \dots, c_{i,n}]^T \in \mathbb{R}^n$ and w_i are the center and width of the Gaussian function, respectively.

Lemma 4. (Hardy et al., 1952) For any $z_1 \in \mathbb{R}$, $z_2 \in \mathbb{R}$, and $0 < p < 1$, the following inequality holds:

$$(|z_1| + |z_2|)^p \leq |z_1|^p + |z_2|^p. \quad (17)$$

Lemma 5. (Hardy et al., 1952) For any $z_1 \in \mathbb{R}$, $z_2 \in \mathbb{R}$, $p > 0$, $q > 0$, and $\xi > 0$, the following inequality holds:

$$|z_1|^p |z_2|^q \leq \frac{p}{p+q} \xi |z_1|^{p+q} + \frac{q}{p+q} \xi^{-\frac{p}{q}} |z_2|^{p+q}. \quad (18)$$

Lemma 6. (Hardy et al., 1952) For any $z_1 \in \mathbb{R}$, $z_2 \in \mathbb{R}$, $0 < p = p_1/p_2 \leq 1$, where p_1 and p_2 are positive odd integers, the following inequality holds:

$$|z_1^p - z_2^p| \leq 2^{1-p} |z_1 - z_2|^p. \quad (19)$$

3. Control design and stability argument

3.1. Control design

For system (12), the new type of finite-time integral sliding mode surface is constructed as

$$s = x_2 + \int_0^t l_2 (x_2^p(\tau) + l_1^p x_1(\tau))^{\frac{2}{p}-1} d\tau, \quad (20)$$

where $1 < p = p_1/p_2 < 2$, p_1 and p_2 are positive odd integers, and the design parameters l_1 and l_2 are selected satisfying the following conditions:

$$l_1 \geq \frac{2^{1-\frac{1}{p}} p + 1}{1+p} + 2^{-\frac{1+p}{2p}} \kappa, \quad (21)$$

$$\begin{aligned} l_2 \geq & 2^{2-\frac{2}{p}} \left(2 - \frac{1}{p} \right) l_1^p + \frac{2^{1-\frac{1}{p}}}{(1+p)} \left(2 - \frac{1}{p} \right) \left(2^{1-\frac{1}{p}} + p \right) l_1^{p+1} \\ & + 2^{1-\frac{1}{p}} \left(2 - \frac{1}{p} \right)^{\frac{p-1}{2p}} l_1^{\frac{p^2-1}{2p}} \kappa, \end{aligned} \quad (22)$$

where $\kappa > 0$. Then, the time differentiation of s can be evaluated as

$$\begin{aligned}\dot{s} &= \dot{x}_2 + l_2(x_2^p + l_1^p x_1)^{\frac{2}{p}-1} \\ &= Hu_c + F + \delta + l_2(x_2^p + l_1^p x_1)^{\frac{2}{p}-1}.\end{aligned}\quad (23)$$

The NN is introduced to identify the lumped uncertainty δ . Define the variable $\mathbf{Z} = [x_1, x_2, u_c]^T$. According to Lemma 3, the lumped uncertainty can be expressed as

$$\delta = \mathbf{W}^{*T} \Phi(\mathbf{Z}) + \varepsilon(\mathbf{Z}), \quad (24)$$

where $\mathbf{W}^* \in \mathbb{R}^N$ is the optimal RBFNN weight, $\Phi(\mathbf{Z}) \in \mathbb{R}^N$ is the basis function vector, $\varepsilon(\mathbf{Z})$ is the identification error satisfying $|\varepsilon(\mathbf{Z})| \leq \bar{\varepsilon}$, $\bar{\varepsilon} > 0$, and N is the number of neurons. Substituting $\|\mathbf{W}^*\| \leq \bar{W}$ into (24), we have

$$|\delta| \leq \|\mathbf{W}^*\| \|\Phi(\mathbf{Z})\| + |\varepsilon(\mathbf{Z})| \leq b\Phi, \quad (25)$$

where $b = \max\{\bar{W}, \bar{\varepsilon}\}$ is an unknown constant and $\Phi = \|\Phi(\mathbf{Z})\| + 1$ is a known function. Then, based on the integral sliding mode surface (20), the indirect neural-based finite-time integral sliding mode controller is developed as

$$u_c = \frac{1}{H} \left(-k_1 s - k_2 \text{sig}^q(s) - l_2(x_2^p + l_1^p x_1)^{\frac{2}{p}-1} - F - \frac{\hat{b}_s \Phi^2 s}{2\eta^2} \right), \quad (26)$$

where $k_1 > 0$, $k_2 > 0$, $0 < q < 1$, $\eta > 0$, \hat{b}_s is the estimation of $b_s = b^2$, and the symbol $\text{sig}^p(\cdot)$ is defined as $\text{sig}^p(z) = |z|^p \text{sgn}(z)$. Moreover, the parametric adaptive learning law is designed as

$$\dot{\hat{b}}_s = -\xi_1 \hat{b}_s + \xi_2 \frac{\Phi^2 s^2}{2\eta^2}, \quad (27)$$

where $\xi_1 > 0$ and $\xi_2 > 0$.

3.2. Stability argument

Then, the practical finite-time stability of the whole closed-loop system can be strictly achieved through the following main theorem.

Theorem 1. Suppose the Mars entry vehicle under aerodynamic and density uncertainties. If we employ the indirect neural-based finite-time integral sliding mode controller (26) and the parametric adaptive learning law (27), then the whole closed-loop system is practically finite-time stable, and the radial distance tracking error x_1 and its time differentiation x_2 can regulate to the small residual sets around zero in finite time.

Proof. The proof involves two steps: arriving phase and sliding phase. In the arriving phase, we will prove that under the proposed controller u_c , the integral sliding mode surface s can regulate to the small residual set around zero in finite time. In the sliding phase, we will prove that when the integral sliding mode surface arrives to zero, the radial distance tracking error x_1 and its time differentiation x_2 can regulate to zero in finite time.

Step 1: arriving phase.

Suppose the following Lyapunov function:

$$V_1 = \frac{1}{2} s^2 + \frac{1}{2\xi_2} \tilde{b}_s^2, \quad (28)$$

where $\tilde{b}_s = b_s - \hat{b}_s$ is the estimation error of b_s . The time differentiation of V_1 can be evaluated as

$$\begin{aligned}\dot{V}_1 &= s\dot{s} - \frac{1}{\xi_2} \tilde{b}_s \dot{\hat{b}}_s \\ &= s(Hu_c + F + \delta + l_2(x_2^p + l_1^p x_1)^{\frac{2}{p}-1}) - \frac{1}{\xi_2} \tilde{b}_s \dot{\hat{b}}_s.\end{aligned}\quad (29)$$

Substituting the indirect neural-based finite-time integral sliding mode controller (26) and the parametric adaptive learning law (27) into (29), we have

$$\begin{aligned}\dot{V}_1 &= s \left(-k_1 s - k_2 \text{sig}^q(s) - \frac{\hat{b}_s \Phi^2 s}{2\eta^2} + \delta \right) - \tilde{b}_s \left(-\frac{\xi_1}{\xi_2} \hat{b}_s + \frac{\Phi^2 s^2}{2\eta^2} \right) \\ &= -k_1 s^2 - k_2 |s|^{q+1} - \frac{\hat{b}_s \Phi^2 s^2}{2\eta^2} + s\delta + \frac{\xi_1}{\xi_2} \tilde{b}_s \hat{b}_s.\end{aligned}\quad (30)$$

The following inequalities hold:

$$s\delta \leq \frac{b^2 \Phi^2 s^2}{2\eta^2} + \frac{\eta^2}{2} = \frac{b_s \Phi^2 s^2}{2\eta^2} + \frac{\eta^2}{2}, \quad (31)$$

$$\frac{\xi_1}{\xi_2} \tilde{b}_s \hat{b}_s = \frac{\xi_1}{\xi_2} \tilde{b}_s (b_s - \tilde{b}_s) \leq \frac{\xi_1}{2\xi_2} b_s^2 - \frac{\xi_1}{2\xi_2} \tilde{b}_s^2. \quad (32)$$

Substituting (31) and (32) into (30) and applying Lemma 4, it follows that

$$\begin{aligned}\dot{V}_1 &\leq -k_1 s^2 - k_2 |s|^{q+1} - \frac{\xi_1}{2\xi_2} \tilde{b}_s^2 + \frac{\xi_1}{2\xi_2} b_s^2 + \frac{\eta^2}{2} \\ &\leq -k_1 s^2 - \frac{\xi_1}{2\xi_2} \tilde{b}_s^2 + \frac{\xi_1}{2\xi_2} b_s^2 + \frac{\eta^2}{2} \\ &\leq -\beta V_1 + \varphi,\end{aligned}\quad (33)$$

where $\beta = \min\{2k_1, \xi_1\}$ and $\varphi = \frac{\xi_1}{2\xi_2} b_s^2 + \frac{\eta^2}{2}$. Solving (33), we have

$$V_1 \leq \left(V_1(0) - \frac{\varphi}{\beta} \right) e^{-\beta t} + \frac{\varphi}{\beta}. \quad (34)$$

Combining with the definition of V_1 , we have \tilde{b}_s is bounded with $|\tilde{b}_s| \leq B$ where B is an unknown positive constant.

Then, suppose another Lyapunov function:

$$V_2 = \frac{1}{2} s^2. \quad (35)$$

Similarly, the time differentiation of V_2 can be evaluated as

$$\begin{aligned}\dot{V}_2 &= s\dot{s} \leq -k_1 s^2 - k_2 |s|^{q+1} + \frac{\tilde{b}_s \Phi^2 s^2}{2\eta^2} + \frac{\eta^2}{2} \\ &\leq -k_1 s^2 - k_2 |s|^{q+1} + \frac{B \Phi^2 s^2}{2\eta^2} + \frac{\eta^2}{2} \\ &= -\left(k_1 - \frac{B \Phi^2}{2\eta^2} \right) s^2 - k_2 |s|^{q+1} + \frac{\eta^2}{2} \\ &= -\kappa_1 V_2 - \kappa_2 V_2^{\frac{q+1}{2}} + \vartheta,\end{aligned}\quad (36)$$

where $\kappa_1 = 2k_1 - \frac{B\Phi^2}{\eta^2}$, $\kappa_2 = 2^{\frac{q+1}{2}}k_2$, and $\vartheta = \frac{\eta^2}{2}$. To ensure $\kappa_1 > 0$, the design parameter k_1 should be selected satisfying the following condition:

$$k_1 > \frac{B\Phi^2}{2\eta^2}. \quad (37)$$

Then, by Lemma 2, the whole closed-loop system is practically finite-time stable and V_2 can regulate to the following small residual set around zero in finite time:

$$\mathcal{Q} = \left\{ V_2 \in \mathbb{R} \mid V_2 \leq \frac{\vartheta}{(1-\iota)\kappa_1} \right\}, \quad (38)$$

where $0 < \iota < 1$. Combining with the definition of V_2 , we further have the integral sliding mode surface s can regulate to the small residual set around zero in finite time. Moreover, the upper bound of the finite settling time of the arriving phase is given as

$$T_{\text{arriving}} \leq \frac{2}{\iota\kappa_1(1-q)} \ln \frac{\iota\kappa_1 V_2^{\frac{1-q}{2}}(0) + \kappa_2}{\kappa_2}. \quad (39)$$

Step 2: sliding phase.

Define the intermediate variables $x_2^* = -l_1 x_1^{\frac{1}{p}}$ and $\zeta = x_2^p - x_2^{*p}$. When the integral sliding mode surface arrives to zero, it follows that

$$\begin{cases} \dot{x}_1 = x_2, \\ \dot{x}_2 = -l_2 \zeta^{\frac{2-p}{p}-1}. \end{cases} \quad (40)$$

Suppose the following Lyapunov function:

$$L = L_1 + L_2, \quad (41)$$

where L_1 and L_2 are defined as

$$L_1 = \frac{1}{2} x_1^2, \quad (42)$$

$$L_2 = \frac{1}{2^{1-\frac{1}{p}}(2-\frac{1}{p})l_1^{1+p}} \int_{x_2^*}^{x_2} (\chi^p - x_2^{*p})^{2-\frac{1}{p}} d\chi. \quad (43)$$

Applying Lemmas 5 and 6, the time differentiation of L_1 can be evaluated as

$$\begin{aligned} \dot{L}_1 &= x_1 x_2 = x_1 x_2^* + x_1 (x_2 - x_2^*) \\ &\leq -l_1 x_1^{1+\frac{1}{p}} + 2^{1-\frac{1}{p}} |x_1| |\zeta|^{\frac{1}{p}} \\ &\leq -\left(l_1 - \frac{2^{1-\frac{1}{p}}}{1+p}\right) |x_1|^{1+\frac{1}{p}} + \frac{2^{1-\frac{1}{p}}}{1+p} |\zeta|^{1+\frac{1}{p}}. \end{aligned} \quad (44)$$

Applying Lemmas 5 and 6, the time differentiation of L_2 can be evaluated as

$$\begin{aligned} \dot{L}_2 &= \frac{x_2}{2^{1-\frac{1}{p}}l_1} \int_{x_2^*}^{x_2} (\chi^p - x_2^{*p})^{1-\frac{1}{p}} d\chi + \frac{1}{2^{1-\frac{1}{p}}(2-\frac{1}{p})l_1^{1+p}} \zeta^{2-\frac{1}{p}} \dot{\zeta} \\ &\leq \frac{1}{2^{1-\frac{1}{p}}l_1} |x_2| |x_2 - x_2^*| |\zeta|^{1-\frac{1}{p}} + \frac{1}{2^{1-\frac{1}{p}}(2-\frac{1}{p})l_1^{1+p}} \zeta^{2-\frac{1}{p}} \dot{\zeta} \\ &\leq \frac{1}{l_1} |x_2| |\zeta| + \frac{1}{2^{1-\frac{1}{p}}(2-\frac{1}{p})l_1^{1+p}} \zeta^{2-\frac{1}{p}} \dot{\zeta} \end{aligned}$$

$$\begin{aligned} &\leq \frac{1}{l_1} |\zeta| |x_2 - x_2^*| + \frac{1}{l_1} |\zeta| |x_2^*| + \frac{1}{2^{1-\frac{1}{p}}(2-\frac{1}{p})l_1^{1+p}} \zeta^{2-\frac{1}{p}} \dot{\zeta} \\ &\leq \frac{1}{l_1} 2^{1-\frac{1}{p}} |\zeta|^{1+\frac{1}{p}} + |\zeta| |x_1|^{\frac{1}{p}} + \frac{1}{2^{1-\frac{1}{p}}(2-\frac{1}{p})l_1^{1+p}} \zeta^{2-\frac{1}{p}} \dot{\zeta} \\ &\leq \left(\frac{2^{1-\frac{1}{p}}}{l_1} + \frac{p}{1+p}\right) |\zeta|^{1+\frac{1}{p}} + \frac{1}{1+p} |x_1|^{1+\frac{1}{p}} \\ &\quad + \frac{1}{2^{1-\frac{1}{p}}(2-\frac{1}{p})l_1^{1+p}} \zeta^{2-\frac{1}{p}} \dot{\zeta}. \end{aligned} \quad (45)$$

Subsequently, the time differentiation of L can be evaluated as

$$\begin{aligned} \dot{L} &= \dot{L}_1 + \dot{L}_2 \\ &\leq -\left(l_1 - \frac{2^{1-\frac{1}{p}}p+1}{1+p}\right) |x_1|^{1+\frac{1}{p}} + \left(\frac{2^{1-\frac{1}{p}}p}{1+p} + \frac{2^{1-\frac{1}{p}}}{l_1}\right) |\zeta|^{1+\frac{1}{p}} \\ &\quad + \frac{1}{2^{1-\frac{1}{p}}(2-\frac{1}{p})l_1^{1+p}} \zeta^{2-\frac{1}{p}} \dot{\zeta}. \end{aligned} \quad (46)$$

Substituting (40) into (46), we have

$$\begin{aligned} \dot{L} &\leq -\left(l_1 - \frac{2^{1-\frac{1}{p}}p+1}{1+p}\right) |x_1|^{1+\frac{1}{p}} \\ &\quad - \left(-\frac{2^{1-\frac{1}{p}}p}{1+p} - \frac{2^{1-\frac{1}{p}}}{l_1} + \frac{l_2}{2^{1-\frac{1}{p}}(2-\frac{1}{p})l_1^{1+p}}\right) |\zeta|^{1+\frac{1}{p}}. \end{aligned} \quad (47)$$

On the other hand, applying Lemma 6 to (41), it follows that

$$L_2 \leq \frac{1}{2^{1-\frac{1}{p}}(2-\frac{1}{p})l_1^{1+p}} |x_2 - x_2^*| |\zeta|^{2-\frac{1}{p}} \leq \frac{1}{(2-\frac{1}{p})l_1^{1+p}} \zeta^2. \quad (48)$$

Substituting (48) into (41) and applying Lemma 4, we have

$$\begin{aligned} L^{\frac{1+p}{2p}} &\leq \left(\frac{1}{2} x_1^2 + \frac{1}{(2-\frac{1}{p})l_1^{1+p}} \zeta^2\right)^{\frac{1+p}{2p}} \\ &\leq \frac{1}{2^{\frac{1+p}{2p}}} |x_1|^{1+\frac{1}{p}} + \frac{1}{(2-\frac{1}{p})^{\frac{1+p}{2p}} l_1^{\frac{(1+p)^2}{2p}}} |\zeta|^{1+\frac{1}{p}}. \end{aligned} \quad (49)$$

Combining (47) and (49) and substituting the conditions (21) and (22) into it, we further have

$$\dot{L} + \kappa L^{\frac{1+p}{2p}} \leq 0. \quad (50)$$

Then, by Lemma 1, system (40) is globally finite-time stable and L can regulate to zero in finite time. Moreover, the upper bound of the finite settling time of the sliding phase is given as

$$T_{\text{sliding}} \leq \frac{2L^{\frac{p-1}{2p}}(0)}{\kappa(p-1)}. \quad (51)$$

Combining with the definition of L , we further have the radial distance tracking error x_1 and its time differentiation x_2 can regulate to the small residual sets around zero in finite time.

From the results of Steps 1 and 2, under the proposed controller u_c , the integral sliding mode surface s can regulate to the small residual set around zero in finite time. Moreover, when the integral sliding mode surface arrives to zero, the radial distance tracking error x_1 and its time differentiation x_2 can regulate to zero in finite time. Consequently, we have that the whole closed-loop system is practically finite-time stable and the radial distance tracking error x_1 and its time differentiation x_2 can regulate to the small residual sets around zero in finite time. Moreover, the upper bound of the finite settling time is given as $T_{total} \leq \max \{T_{arriving}, T_{sliding}\}$. The proof is thus completed. ■

Remark 1. Different from the terminal sliding mode surface in Dai and Xia (2015), Zhao et al. (2015), Dai et al. (2017), Shen et al. (2018a, 2018b, 2019), Gong et al. (2020), and Long et al. (2020) and the integral sliding mode surface based on the homogeneous method in Zhao et al. (2016), the proposed finite-time integral sliding mode surface (20) is constructed based on the adding a power integrator technique. Benefiting from the new type of finite-time integral sliding mode surface, the finite-time integral sliding mode controller has no singularity problem, which overcomes a major drawback of the conventional terminal sliding mode control.

Remark 2. For the conventional neural or fuzzy identification in Li and Peng (2012b), Li and Jiang (2015), Huang et al. (2019), and Li et al. (2019), the number of adaptive learning parameters that needed to be adjusted online is N . Alternatively, the concept of indirect neural identification (27) is introduced in this work and thus the computation burden of the proposed controller is heavily reduced. This makes the proposed controller more suitable for practical engineering especially considering the onboard computer of the Mars entry vehicle usually has the limited computational capability.

Remark 3. Some advises are provided to tune the design parameters of the proposed controller. Note that l_1 , l_2 , k_1 , k_2 , ξ_1 , and ξ_2 are key parameters. Large l_1 , l_2 , k_1 , k_2 , ξ_1 , and ξ_2 can result in the relatively high tracking accuracy and fast convergence speed. However, large l_1 , l_2 , k_1 , and k_2 can also lead to the relatively large bank angle control command. The deviation between the control command and the input constraint cannot be too large in practical applications. Moreover, large ξ_1 and ξ_2 can in turn induce the relatively poor transient response. From this point of view, the design parameters of the proposed controller should be properly selected by trial and error to realize the satisfactory guidance performance.

Remark 4. For convenience of the readers to have a better understanding, the block diagram of the proposed indirect neural-based finite-time integral sliding mode controller is depicted in Fig. 1. Actually, the proposed controller is developed as a combination of finite-time integral sliding mode controller and indirect neural identification.

4. Simulation studies

In this section, simulation studies are provided on a Mars Science Laboratory-type (MSL-type) entry vehicle (Mendeck and McGrew, 2014; Benito and Mease, 2010) to illustrate the proposed control algorithm. The fundamental parameters of the Mars and the entry vehicle are given in Table 1. Moreover, the initial states of the entry vehicle are presented in Table 2. The reference trajectory is generated by conducting a simulation under the nominal case with a constant bank angle of 59.63 deg. The control command is updated each second and the guidance breaks off when the entry vehicle arrives to the parachute opening altitude.

The following simulations can be divided into two scenarios. Scenario 1 is the performance comparisons by comparing the proposed controller with two existing controllers. Moreover, Scenario 2 is the Monte Carlo simulations to further test the robustness and parachute opening point precision of the proposed controller.

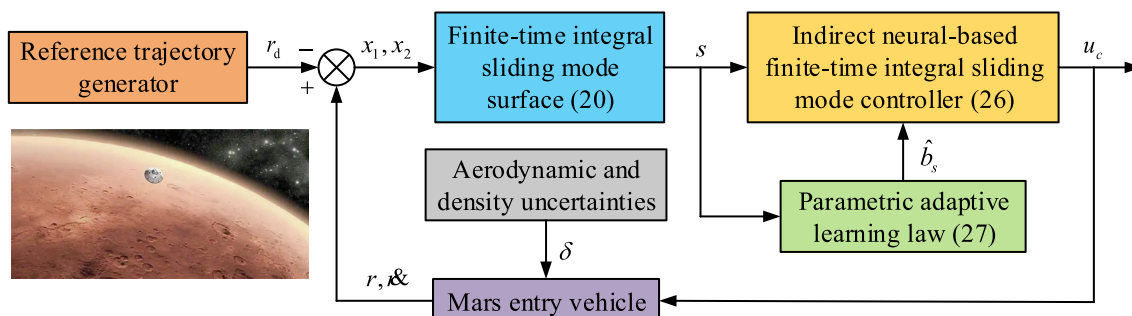


Fig. 1. Structure of the proposed control algorithm.

4.1. Performance comparisons

In Scenario 1, performance comparisons are carried out by comparing the proposed controller with two existing controllers. In the simulations, the aerodynamic and density uncertainties are set as $\Delta C_L = 0.15 \cos(\pi t/15)C_{L0}$, $\Delta C_D = 0.1 \sin(\pi t/18)C_{D0}$, and $\Delta \rho = 0.12 \sin(\pi t/12)\rho_0$. Moreover, the initial state deviations are given as $\bar{h}_0 = h_0 + 0.01$ km and $\bar{V}_0 = V_0 + 1$ m/s. In addition to the proposed indirect neural-based finite-time integral sliding mode controller (26), the finite-time PD controller in Hong et al. (2002) and the fast terminal sliding mode controller in Yu et al. (2005) are also employed for performance comparisons. Specifically, the finite-time PD controller in Hong et al. (2002) is given as

$$u_c = \frac{1}{H}(-k_1 \text{sig}^p(x_1) - k_2 \text{sig}^q(x_2) - F), \quad (52)$$

where $k_1 > 0$, $k_2 > 0$, $0 < p < 1$, and $q = 2p/(p+1)$. For the fast terminal sliding mode controller in Yu et al. (2005), the fast terminal sliding mode surface is constructed as

$$s = x_2 + l_1 x_1 + l_2 \text{sig}^p(x_1), \quad (53)$$

where $l_1 > 0$, $l_2 > 0$, and $0 < p < 1$. Then, the fast terminal sliding mode controller is designed as

$$u_c = \frac{1}{H}(-k_1 s - k_2 \text{sig}^q(s) - l_1 x_2 - l_2 p |x_1|^{p-1} x_2 - F - \eta \text{sgn}(s)), \quad (54)$$

where $k_1 > 0$, $k_2 > 0$, $0 < q < 1$, and $\eta > 0$.

The parameters of the proposed controller (26) are selected as $l_1 = 1.2$, $l_2 = 3$, $p = 101/99$, $k_1 = 5$, $k_2 = 5$, $q = 99/101$, $\xi_1 = 0.1$, $\xi_2 = 1$, and $\eta = 0.1$. Seven nodes are provided for the hidden layer of the RBFNN. The

Table 1
Fundamental parameters of the Mars and the entry vehicle.

Parameter	Value
Mass of the entry vehicle m (kg)	2804
Reference area of the entry vehicle S (m ²)	15.39
Lift coefficient of the entry vehicle C_L	0.37
Drag coefficient of the entry vehicle C_D	1.37
Mars radius r_M (km)	3396
Martian gravitational constant μ_M (m ³ /s ²)	4.2828×10^{13}
Atmospheric density on Martian surface ρ_s (kg/m ³)	0.0158
Scale altitude for Martian atmospheric density h_s (m)	9354

Table 2
Initial states of the entry vehicle.

Parameter	Value
Initial flight altitude of the entry vehicle h_0 (km)	133.56
Initial latitude of the entry vehicle θ_0 (deg)	−90.072
Initial longitude of the entry vehicle λ_0 (deg)	−43.898
Initial velocity of the entry vehicle V_0 (m/s)	5505
Initial flight path angle of the entry vehicle γ_0 (deg)	−14.15
Initial heading angle of the entry vehicle ψ_0 (deg)	4.99

parameters of the RBFNN are selected as $c_i = [-3, -2, -1, 0, 1, 2, 3]^T$ and $w_i = 6$. The initial value of the adaptive parameter is set as $\hat{B}_s(0) = 0$. Moreover, the parameters of the finite-time PD controller (52) are selected as $k_1 = 5$, $k_2 = 5$, $p = 99/101$, and $q = 99/100$. The parameters of the fast terminal sliding mode controller (54) are selected as $l_1 = 1$, $l_2 = 1$, $p = 99/101$, $k_1 = 2$, $k_2 = 2$, $q = 99/101$, and $\eta = 0.1$.

The simulation results are provided in Figs. 2–6. Specifically, Figs. 2 and 3 show the time profiles of the altitude tracking and velocity tracking, respectively. It is clearly seen that the proposed controller and two compared controllers can realize the reference trajectory tracking guidance with success. Moreover, the time profile of the radial distance tracking error is presented in Fig. 4. It is not difficult to find that the proposed controller can achieve the more excellent guidance performance associated with higher steady-state radial distance tracking accuracy. By contrast, the guidance performances of the finite-time PD-like controller and the fast terminal sliding mode controller are relatively poor due to the existence of aerodynamic and density uncertainties. Fig. 5 gives the time profile of the bank angle control command. The time profile of the adaptive parameter is shown in Fig. 6. It is obvious that the adaptive parameter is changing with time smoothly. Benefiting from the indirect neural identification, the proposed controller is strongly robust against aerodynamic and density uncertainties. Moreover, only a single adaptive parameter is required to be learned online, which makes the proposed controller computationally simple for onboard implementations.

Furthermore, for quantitative performance comparisons between the proposed controller and two compared controllers, the integrated absolute error (IAE) and integrated time absolute error (ITAE) of these controllers are listed in Table 3. The IAE and ITAE are defined as $IAE = \int_0^t |x_1(\tau)| d\tau$ and $ITAE = \int_0^t \tau |x_1(\tau)| d\tau$, respectively,

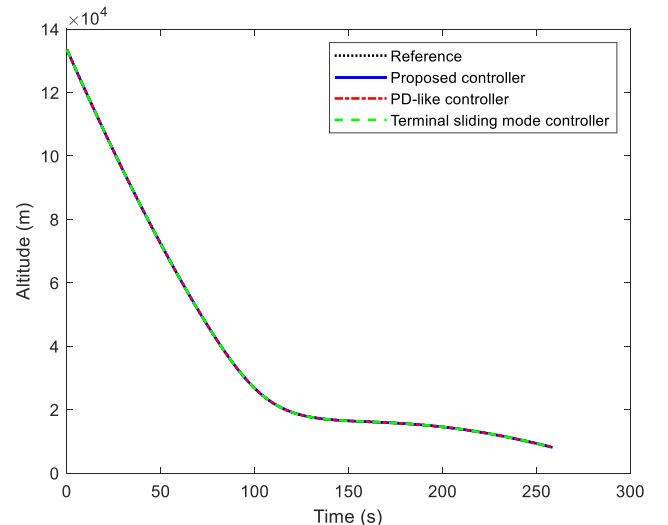


Fig. 2. Time profile of the altitude tracking.

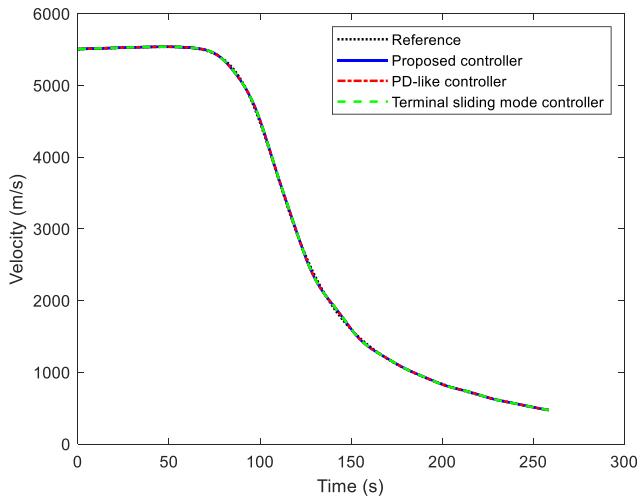


Fig. 3. Time profile of the velocity tracking.

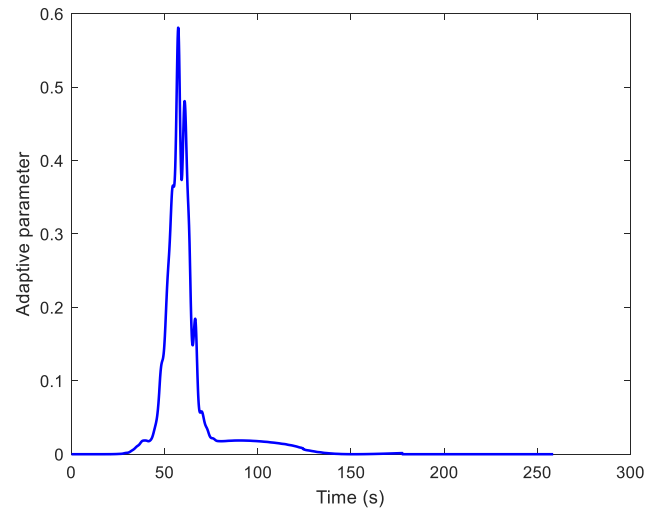


Fig. 6. Time profile of the adaptive parameter.

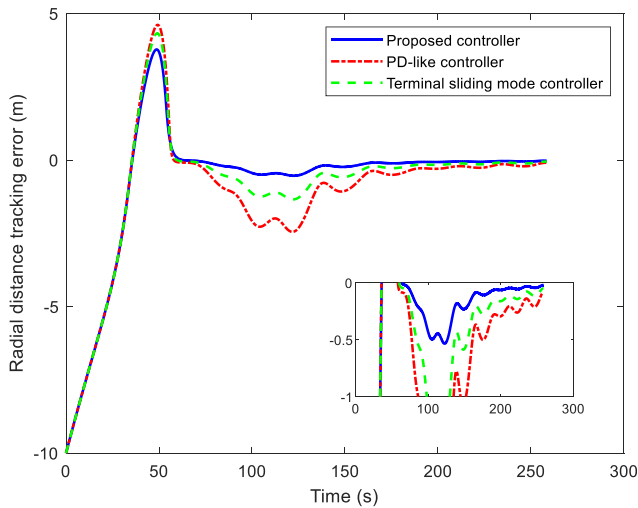


Fig. 4. Time profile of the radial distance tracking error.

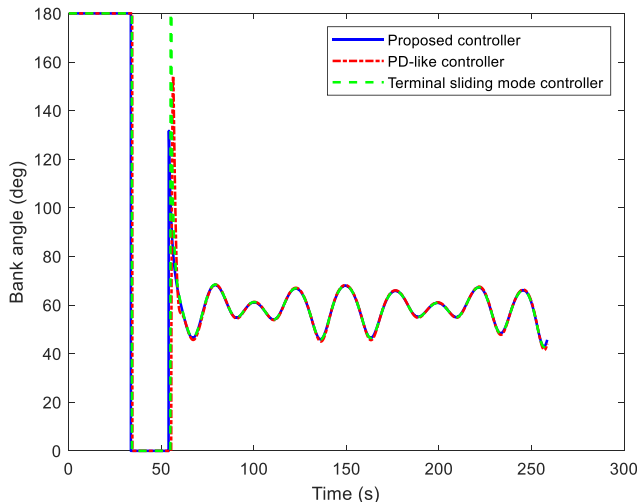


Fig. 5. Time profile of the bank angle control command.

which correspond to the steady-state and transient performance of the controllers to some degree. From Table 3, it is not difficult to find that the IAE and ITAE of two compared controllers are much larger than those of the proposed controller, which means the proposed controller possesses the better steady-state and transient performance than the finite-time PD-like controller and the fast terminal sliding mode controller.

In summary, the proposed control algorithm is able to achieve the more excellent guidance performance and higher uncertainty rejection capability in the presence of aerodynamic and density uncertainties and initial state deviations than the finite-time PD-like controller and the fast terminal sliding mode controller.

4.2. Monte Carlo simulations

In Scenario 2, a total number of 1000 runs Monte Carlo simulations are provided to further test the robustness and parachute opening point precision of the proposed controller. In the Monte Carlo simulations, the initial altitude deviation is considered to be uniformly distributed in $[-0.01, 0.01]$ km and the initial velocity deviation is considered to be uniformly distributed in $[-1, 1]$ m/s. Moreover, the lift and drag coefficient uncertainties ΔC_L and ΔC_D are set to be normally distributed in $[-20\%, 20\%]$ and the density uncertainty $\Delta \rho$ is set to be normally distributed in $[-10\%, 10\%]$ with respect to their nominal values. The control parameters of the proposed controller and the two

Table 3
IAE and ITAE of the proposed controller and two compared controllers.

Controller	IAE	ITAE
Proposed controller	159.4	6868.6
Finite-time PD-like controller	207.8	12657.3
Fast terminal sliding mode controller	171.7	8130.6

compared controllers are selected the same as those in Scenario 1.

The parachute opening position distributions under the proposed controller and two compared controllers are given as Figs. 7–9, respectively. It is obvious that the proposed controller can realize the higher parachute opening point accuracy than the finite-time PD-like controller and the fast terminal sliding mode controller. Specifically, under the proposed controller, the 100% runs parachute opening positions are within the 10 km error ellipse and the 98.3% runs parachute opening positions are within the 5 km error ellipse. By contrast, under the finite-time PD-like controller, the 98.2% runs parachute opening positions are within the 10 km error ellipse and the 42.2% runs parachute opening positions are within the 5 km error ellipse. Moreover, under the fast terminal sliding mode controller, the 100% runs parachute opening positions are within the 10 km error ellipse and the 65.4% runs parachute opening positions are within the 5 km error ellipse. It

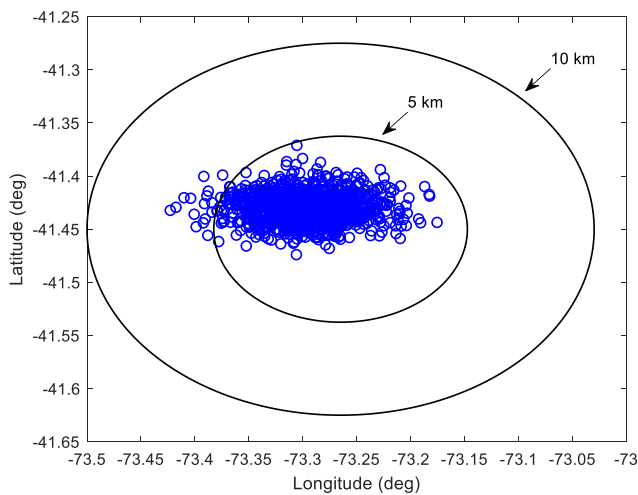


Fig. 7. Parachute opening position distribution under the proposed controller.

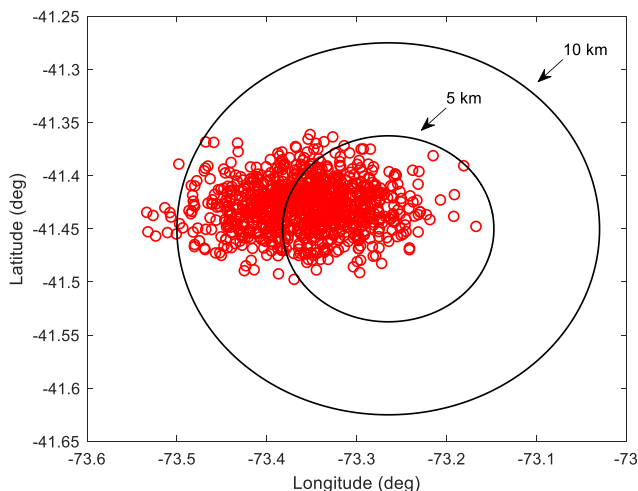


Fig. 8. Parachute opening position distribution under the PD controller.

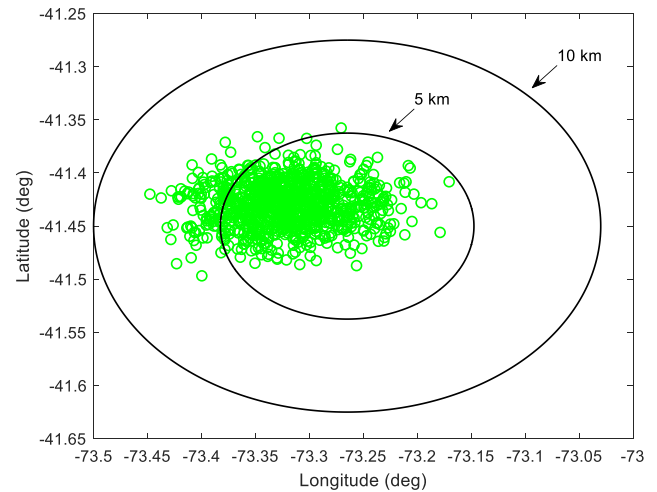


Fig. 9. Parachute opening position distribution under the sliding mode controller.

should be pointed out that the parachute opening position deviations are mainly caused by the aerodynamic and density uncertainties and initial state deviations. Thus, the Monte Carlo simulation results indicate that the proposed controller has the higher parachute opening point precision and stronger robustness against aerodynamic and density uncertainties and initial state deviations than the finite-time PD-like controller and the fast terminal sliding mode controller.

5. Conclusion

In this article, an indirect neural-based finite-time integral sliding mode control algorithm is presented for the reference trajectory tracking guidance of Mars entry vehicle under uncertainties. The proposed controller is developed as a combination of finite-time integral sliding mode controller and indirect neural identification. A new type of finite-time integral sliding mode surface is constructed, based on which the finite-time integral sliding mode controller is designed with no singularity problem. Moreover, the NN is combined to identify the lumped uncertainty by introducing the concept of indirect neural identification. In this way, only a single adaptive parameter is required to be learned online and thus the proposed controller is computationally simple for onboard implementations. Lastly, simulation results indicate that the proposed control algorithm can achieve the excellent guidance performance associated with high parachute opening point precision and strong robustness against aerodynamic and density uncertainties and initial state deviations. It is expected that the proposed control algorithm can provide the beneficial theoretical support to the entry vehicle guidance system design for future manned Mars exploration and sample-return missions. Inspired by Shen et al. (2020) and Yao et al. (2022), we will attempt to improve the proposed controller

to the fixed-time convergence scenario in our future research.

Declaration of Competing Interest

The authors declare that they have no known competing financial interests or personal relationships that could have appeared to influence the work reported in this paper.

Acknowledgment

The Deanship of Scientific Research (DSR) at King Abdulaziz University, Jeddah, Saudi Arabia has funded this project, under grant no. (RG-3-611-43).

References

- Benito, J., Mease, K.D., 2010. Reachable and controllable sets for planetary entry and landing. *J. Guid. Control Dyn.* 33 (3), 641–654.
- Bharadwaj, S., Rao, A.V., Mease, K.D., 1998. Entry trajectory tracking law via feedback linearization. *J. Guid. Control Dyn.* 21 (5), 726–732.
- Bhat, S.P., Bernstein, D.S., 2000. Finite-time stability of continuous autonomous systems. *SIAM J. Control Optim.* 38 (3), 751–766.
- Braun, R.D., Manning, R.M., 2007. Mars exploration entry, descent, and landing challenges. *J. Spacecr. Rockets* 44 (2), 310–323.
- Dai, J., Gao, A., Xia, Y., 2017. Mars atmospheric entry guidance for reference trajectory tracking based on robust nonlinear compound controller. *Acta Astronaut.* 132, 221–229.
- Dai, J., Xia, Y., 2015. Mars atmospheric entry guidance for reference trajectory tracking. *Aerosp. Sci. Technol.* 45, 335–345.
- Gong, Y., Guo, Y., Ma, G., Guo, M., 2020. Mars entry guidance for mid-lift-to-drag ratio vehicle with control constraints. *Aerosp. Sci. Technol.* 107 106361.
- Hardy, G.H., Littlewood, J.E., Pólya, G., 1952. *Inequalities*. Cambridge University Press, Cambridge.
- Hong, Y., Xu, Y., Huang, J., 2002. Finite-time control for robot manipulators. *Syst. Control Lett.* 46 (4), 243–253.
- Huang, Y., Li, S., Sun, J., 2019. Mars entry fault-tolerant control via neural network and structure adaptive model inversion. *Adv. Space Res.* 63 (1), 557–571.
- Izzo, D., Märten, M., Pan, B., 2019. A survey on artificial intelligence trends in spacecraft guidance dynamics and control. *Astrodynamics* 3 (4), 287–299.
- Kluever, C.A., 2008. Entry guidance performance for Mars precision landing. *J. Guid. Control Dyn.* 31 (6), 1537–1544.
- Li, T., Dai, Z., Song, G., Wang, L., Du, H., 2019. Fault tolerant tracking of Mars entry vehicles via fuzzy control approach. *Fuzzy Sets Syst.* 371, 123–135.
- Li, S., Jiang, X., 2014. Review and prospect of guidance and control for Mars atmospheric entry. *Prog. Aersp. Sci.* 69, 40–57.
- Li, S., Jiang, X., 2015. RBF neural network based second-order sliding mode guidance for Mars entry under uncertainties. *Aerosp. Sci. Technol.* 43, 226–235.
- Li, S., Peng, Y., 2012a. Command generator tracker based direct model reference adaptive tracking guidance for Mars atmospheric entry. *Adv. Space Res.* 49 (1), 49–63.
- Li, S., Peng, Y.-M., 2012b. Neural network-based sliding mode variable structure control for Mars entry. *Proc. Inst. Mech. Eng., Part G: J. Aerosp. Eng.* 226 (11), 1373–1386.
- Long, J., Zhu, S., Cui, P., Liang, Z., 2020. Barrier Lyapunov function based sliding mode control for Mars atmospheric entry trajectory tracking with input saturation constraint. *Aerosp. Sci. Technol.* 106 106213.
- Lu, P., 2008. Predictor-corrector entry guidance for low-lifting vehicles. *J. Guid. Control Dyn.* 31 (4), 1067–1075.
- Lu, P., 2014. Entry guidance: a unified method. *J. Guid. Control Dyn.* 37 (3), 713–728.
- Lu, K., Xia, Y., Shen, G., Yu, C., Zhou, L., Zhang, L., 2017. Sliding mode control for Mars entry based on extended state observer. *Adv. Space Res.* 60 (9), 2009–2020.
- Mendeck, G.F., McGrew, L.C., 2014. Entry guidance design and postflight performance for 2011 Mars Science Laboratory mission. *J. Spacecr. Rockets* 51 (4), 1094–1105.
- Sanner, R.M., Slotine, J.-J.-E., 1992. Gaussian networks for direct adaptive control. *IEEE Trans. Neural Netw.* 3 (6), 837–863.
- Shen, G., Xia, Y., Zhang, J., Cui, B., 2018a. Finite-time trajectory tracking control for entry guidance. *Int. J. Robust Nonlinear Control* 28 (18), 5895–5914.
- Shen, G., Xia, Y., Zhang, L., Zhang, J., Cui, B., 2018b. A new compound control for Mars entry guidance. *Adv. Space Res.* 62 (1), 580–592.
- Shen, G., Xia, Y., Ma, D., Zhang, J., 2019. Adaptive sliding-mode control for Mars entry trajectory tracking with finite-time convergence. *Int. J. Robust Nonlinear Control* 29 (5), 1249–1264.
- Shen, G., Xia, Y., Zhang, J., Cui, B., 2020. Adaptive fixed-time trajectory tracking control for Mars entry vehicle. *Nonlinear Dyn.* 102 (4), 2687–2698.
- Shirobokov, M., Trofimov, S., Ovchinnikov, M., 2021. Survey of machine learning techniques in spacecraft control design. *Acta Astronaut.* 186, 87–97.
- Tu, K.Y., Munir, M.S., Mease, K.D., Bayard, D.S., 2000. Drag-based predictive tracking guidance for Mars precision landing. *J. Guid. Control Dyn.* 23 (4), 620–628.
- Xia, Y., Chen, R., Pu, F., Dai, L., 2014. Active disturbance rejection control for drag tracking in Mars entry guidance. *Adv. Space Res.* 53 (5), 853–861.
- Xia, Y., Shen, G., Zhou, L., Sun, H., 2015. Mars entry guidance based on segmented guidance predictor-corrector algorithm. *Control Eng. Pract.* 45, 79–85.
- Yan, X., Lyu, S., 2019. Mars entry guidance based on nonlinear model predictive control with disturbance observer. *J. Franklin Inst.* 356 (16), 9824–9843.
- Yao, Q., 2020. Adaptive finite-time sliding mode control design for finite-time fault-tolerant trajectory tracking of marine vehicles with input saturation. *J. Franklin Inst.* 357 (18), 13593–13619.
- Yao, Q., Han, H., Qiao, D., 2022. Nonsingular fixed-time tracking guidance for Mars aerocapture with neural compensation. *IEEE Trans. Aerosp. Electron. Syst.* 58 (4), 3686–3696.
- Yu, Z., Cui, P., Crassidis, J.L., 2014. Design and optimization of navigation and guidance techniques for Mars pinpoint landing: review and prospect. *Prog. Aersp. Sci.* 94, 82–94.
- Yu, S., Yu, X., Shirinzadeh, B., Man, Z., 2005. Continuous finite-time control for robotic manipulators with terminal sliding mode. *Automatica* 41 (11), 1957–1964.
- Zhao, Z., Yang, J., Li, S., Zhang, Z., Guo, L., 2015. Finite-time super-twisting sliding mode control for Mars entry trajectory tracking. *J. Franklin Inst.* 352 (11), 5226–5248.
- Zhao, Z., Yang, J., Li, S., Guo, L., 2016. Drag-based composite super-twisting sliding mode control law design for Mars entry guidance. *Adv. Space Res.* 57 (12), 2508–2518.
- Zheng, Y., 2019. Mars entry guidance using a semi-analytical method. *Adv. Space Res.* 63 (5), 1566–1575.
- Zheng, Y., Cui, H., 2015. Disturbance observer-based robust guidance for Mars atmospheric entry with input saturation. *Chin. J. Aeronaut.* 28 (3), 845–852.
- Zheng, Y., Cui, H., Ai, Y., 2017. Constrained numerical predictor-corrector guidance for Mars precision landing. *J. Guid. Control Dyn.* 40 (1), 177–185.